Journal of Natural Gas Science and Engineering 65 (2019) 275–283

Contents lists available at ScienceDirect

Journal of Natural Gas Science and Engineering

journal homepage: www.elsevier.com/locate/jngse

Staged numerical simulations of supercritical CO_2 fracturing of coal seams based on the extended finite element method

Hao Yan[a,b], Jixiong Zhang[a,b,*], Nan Zhou[a,b], Meng Li[a,b]

[a] State Key Laboratory of Coal Resources and Safe Mining, China University of Mining & Technology, Xuzhou, Jiangsu, 221116, China
[b] School of Mines, China University of Mining & Technology, Xuzhou, Jiangsu, 221116, China

ARTICLE INFO

Keywords:
Supercritical CO_2
Extended finite element method
Staged simulation
Fracturing
Crack propagation

ABSTRACT

As a water-less fracturing mining technology, supercritical CO_2 (SC-CO_2) fracturing has attracted increasing attention in the mining industry. In order to simulate the whole process of SC-CO_2 fracturing and fully understand the fracturing mechanism of SC-CO_2, the thermodynamic analysis method was used to analyze the phase transitions of CO_2 in SC-CO_2 fracturing, and the whole process of SC-CO_2 fracturing was divided into the SC-CO_2 fracturing stage and the CO_2 phase-transition induced fracturing stage. Based on the extended finite element method, the fluid-solid coupling model at the SC-CO_2 fracturing stage, the TNT equivalence of CO_2 phase transition induced fracturing, pressure-time history curves of blast loads, and numerical model of CO_2 phase transition induced fracturing stage were comprehensively analyzed, and the staged numerical simulation method of SC-CO_2 fracturing was proposed. The simulation results showed that cracks in the coal seam were initiated and propagated at the SC-CO_2 fracture stage, and the cracks broadened, and new cracks were generated during the CO_2 phase-transition induced fracturing stage. At the same time, the injection rate of SC-CO2 fluid had a positive impact on its fracturing effect. The larger the injection rate of SC-CO2 fluid, the larger the length and width of crack propagation. This study is of great significance for enriching SC-CO2 fracturing theory.

1. Introduction

In the coal mining industry, the exploitation of coal seams with high gas and low permeability is limited by poor gas drainage efficiency. Coal seams with high mine pressures are limited by severe shock hazards. Hard and thin coal seams are limited by the low lump coal rate (Cao et al., 2017; Xu et al., 2017; Jiang et al., 2016; Dong et al., 2018). Currently, aqueous hydraulic fracturing technologies have been employed widely to circumvent the constraints mentioned above. However, aqueous hydraulic fracturing may cause various issues, including high water consumption, higher costs, and the risk of ground pollution (Estrada and Bhamidimarri, 2016; Camarillo et al., 2016; Luek and Gonsior, 2017; Brownlow et al., 2017; Huang et al., 2014). Supercritical CO_2 (denoted in this article as SC-CO_2) refers to CO_2 fluids with temperatures and pressures above the critical temperature and the critical pressure of CO_2 and they exhibit unique physical and chemical properties (Middleton et al., 2015; Wang et al., 2017a). Combining the low interfacial tension and the high diffusivity of the gas and the high density and good solubility of the fluids, SC-CO_2 has excellent fluidity and transmissibility, and the coal seams demonstrate good permeability to SC-CO_2, so SC-CO_2 is an ideal candidate for fracturing (Er et al., 2010; Vishal, 2017; Zhang et al., 2017a). Compared with hydraulic fracturing, SC-CO_2 fracturing has the following advantages: 1) SC-CO_2 is not flammable and explosive, and will not cause water lock effect and other damage to coal and rock; 2) The initiation pressures of SC-CO_2 is less than that of hydraulic fracturing; 3) SC-CO_2 fluid can easily penetrate into micro-porous cracks, which greatly increases the complexity of crack initiation and propagation, and is more conducive to the formation of complex cracks (Yang et al., 2012; Jia et al., 2018). Therefore, SC-CO_2 fracturing technology has shown good development prospects.

To date, studies of SC-CO_2 fracturing have focused laboratory tests on unconventional oil and gas resources (Wang et al., 2017b). Ishida et al. (2012) investigated SC-CO_2 and CO_2 fluid fracturing of granite and demonstrated that the initiation pressures of SC-CO_2 fluid and CO_2 fluid were reduced compared to those required for aqueous hydraulic fracturing. Zhou et al. (2016) investigated the crack propagation law of SC-CO_2 fracturing of shale with CT, and explored the effects of stress, pore pressure, and gas adsorption on the permeability of shale. Zhang et al. (2017b) analyzed the initiation pressure and crack propagation

* Corresponding author. State Key Laboratory of Coal Resources and Safe Mining, School of Mines, China University of Mining & Technology, Xuzhou, Jiangsu, 221116, China.
E-mail address: zjxiong@cumt.edu.cn (J. Zhang).

https://doi.org/10.1016/j.jngse.2019.03.021
Received 14 October 2018; Received in revised form 22 February 2019; Accepted 21 March 2019
Available online 23 March 2019

law of SC-CO_2 fracturing, and the influence of stratification development on fracturing. Zou et al. (2018) investigated the fracturing of sandstone with significant stratifications, using three fracturing fluids (X guar, water, SC-CO_2) and demonstrated that the use of SC-CO_2 can lead to the merging of natural cracks by increasing the number of stratification cracks and inducing stratification shear failures even under conditions of increasing horizontal stress difference. Although the above scholars conducted a series of experiments and comparisons on SC-CO_2 fracturing, only simple experimental conclusions were given, and the SC-CO_2 fracturing mechanism has not been systematically studied. The analysis of SC-CO_2 fracturing process, the law of crack propagation in SC-CO_2 fracturing process and the influence of various factors on the crack propagation have not been basically studied. At present, the research on SC-CO_2 fracturing technology is still in its infancy, and further research is urgently needed by various methods such as theoretical analysis, laboratory experiments and numerical simulation.

SC-CO_2 fracturing of coal seams is a complicated process involving coal seam-crack-supercritical fluid-gas multi-medium interactions. As SC-CO_2 is highly sensitive to temperature and pressure, phase transitions of CO_2 are observed during the entire fracturing process and the process can be considered being as the SC-CO_2 fracturing stage and the CO_2 phase-transition induced fracturing stage. The CO_2 phase transition induced fracturing stage usually is neglected as it cannot be effectively monitored due to its extremely short duration. Numerical simulations have been employed widely by virtue of their quantitative and visualized results presentation. In the present study, a fluid-solid coupling model was established using the extended finite element method (XFEM) based on the SC-CO_2 fracturing of the coal seam. Additionally, the phase transition energy was regarded as a blast load on the fracturing surface, and a staged numerical simulation method was proposed for SC-CO_2 fracturing of the coal seam. The present study provides a reference for the study of SC-CO_2 fracturing mechanisms.

2. Staged analysis of SC-CO_2 fluid fracturing of coal seams

As a novel fracturing liquid, SC-CO_2 is characterized by excellent fluidity, and transmissibility and it exhibits great advantages for fracturing. Specifically, SC-CO_2 can readily enter micro-pore cracks, resulting in complicated fracturing. In SC-CO_2 fracturing, variations of temperature and pressure may cause severe changes in the properties of the SC-CO_2 fluids, resulting in further complication of the fracturing mechanism (Yang et al., 2018). Therefore, the physical properties of CO_2 during the fracturing process were investigated to understand fully SC-CO_2 fluid fracturing behavior.

The phase transition of CO_2 in SC-CO_2 fracturing is illustrated in Fig. 1 (Martynov et al., 2014). As can be observed, the SC-CO_2 transitions from the supercritical state to the gaseous state and this results in changes in the fracturing mechanism. Hence, the period of SC-CO_2 fracturing is divided into the SC-CO_2 fracturing stage and the CO_2 phase-transition induced fracturing stage.

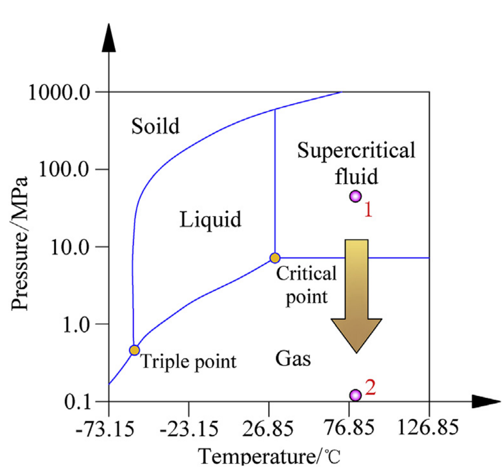

Fig. 1. Phase transition of CO_2 in SC-CO_2 fracturing.

2.1. SC-CO_2 fracturing stage

During the early stage of fracturing, the SC-CO_2 fluid can readily enter micro-pore cracks owing to its low viscosity and high diffusivity, resulting in initiation and propagation of macro-cracks, thus facilitating initiation of complicated crack paths (see Fig. 2). Owing to the low fracturing borehole depth in mining, the temperature remains constant, the fracturing period is relatively short, and heat transfer between the SC-CO_2 and the coal seam is negligible. Hence, it was assumed for the SC-CO_2 fracturing stage that the temperature of SC-CO_2 fluid was constant.

2.2. CO_2 phase-transition induced fracturing stage

During the later stages of fracturing, cracks in the coal seams propagate further, the injection of the SC-CO_2 fluid is suspended, the CO_2 pressure in fracturing holes falls drastically, the SC-CO_2 transitions from the supercritical state to the gaseous state (see "1 → 2" in Fig. 1), and the CO_2 expands sharply in a short time, such that severe impacts led to further fracturing of the cracks in terms of length and width (Zhou et al., 2014; Li et al., 2017) (see Fig. 2). After CO_2 phase-transition induced fracturing, the CO_2 pressure returns to atmospheric pressure.

3. Simulation method and analysis procedures for SC-CO_2 fracturing of coal seams

3.1. Analysis procedures

The numerical simulation of the SC-CO_2 fracturing of coal seams is a complicated process involving coal seam-crack-supercritical fluid-gas multi-medium interactions. Compared to conventional hydraulic fracturing, the SC-CO_2 fracturing process is more complicated and must be simulated in stages. The SC-CO_2 fracturing stage is a fluid-solid coupling process involving the flow of the SC-CO_2 fluid and deformation of the coal seam, while the CO_2 phase-transition induced fracturing stage is a process involving fracturing of the coal seam by the high-pressure CO_2 gas and by its blast impact. The mechanisms of SC-CO_2 fracturing and CO_2 phase-transition induced fracturing of coal seams are highly complicated, so the main innovation of this simulation is to fully reflect the two stages. Several issues require clarification before the simulation details are explained. First, a combination of the SC-CO_2 fracturing process, which takes a longer time, and the CO_2 phase-transition induced fracturing process, which is a transient process. Second, effective establishment of the fluid-solid coupling model for the SC-CO_2 fracturing stage. Third, consideration of the CO_2 phase transition-induced fracturing stage, which is transient in nature and the phase transition energy must be determined.

In the present study, crack propagations during SC-CO_2 fracturing were simulated using XFEM in ABAQUS. A fluid-solid coupling model was developed using the Soil module in ABAQUS for simulation of the SC-CO_2 fracturing stage. Based on that, blast loads induced by phase transition of the CO_2 were introduced into the SC-CO_2 fracturing stage model for simulation of the CO_2 phase-transition induced fracturing stage.

The numerical simulation of SC-CO_2 fracturing of coal seams is illustrated in Fig. 3. The procedures consist of the following four steps:

1) Fluid-solid coupling model for the SC-CO_2 fracturing stage: The fluid-solid coupling model for SC-CO_2 fluids was developed using the XFEM module to investigate crack propagations after the SC-CO_2 fracturing stage.

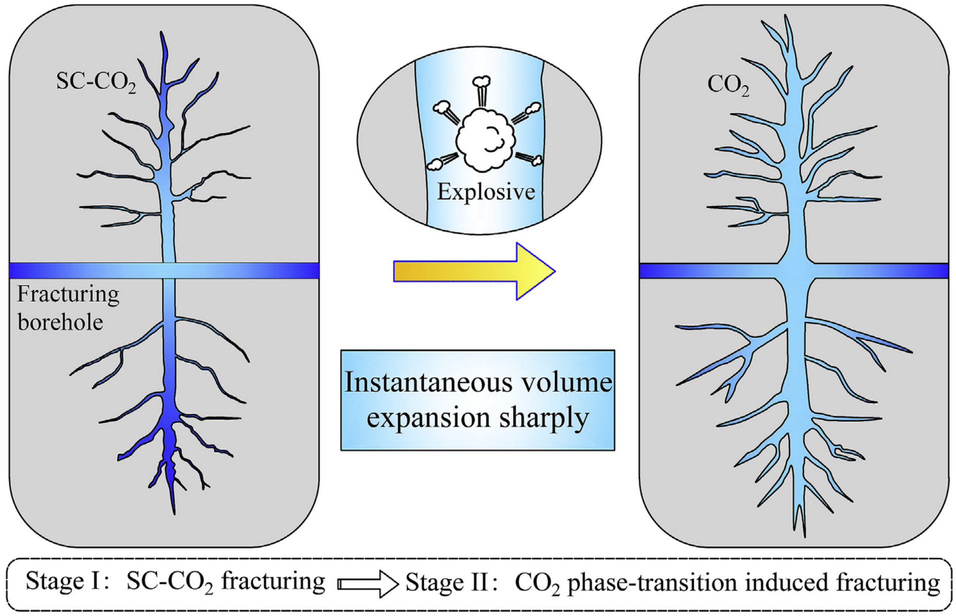

Fig. 2. Characteristics of SC-CO_2 fracturing in different stages.

2) TNT equivalence analysis for the CO_2 phase-transition induced fracturing: Key parameters of cracks in the XFEM simulation at the SC-CO_2 fracturing stage were extracted and the CO_2 phase-transition induced fracturing was calculated and expressed as a TNT equivalence.
3) Pressure-time history curves of blast loads: The pressure-time history curves of blast loads at the borehole wall were obtained by simulation of TNT blasting on AUTODYN.
4) Numerical model for the CO_2 phase-transition induced fracturing stage: Crack propagations after the CO_2 phase-transition induced fracturing stage were investigated by applying the blast load on the fracturing surface.

The first step is to simulate the SC-CO_2 fracturing stage, the forth step is to simulate the CO_2 phase transition-induced fracturing stage, both stages use the XFEM to simulate crack propagation to ensure consistency in simulation studies. The second and the third step is to calculate the equivalent loads of CO_2 phase-transition, so that the fourth step can apply the loads to the crack surface already generated in the first step.

3.2. The fluid-solid coupling model for the SC-CO_2 fracturing stage

The injection of SC-CO_2 fluid into coal seams is indeed a dynamic coupling of the SC-CO_2 flow and the coal seam deformation and its numerical model must consider fluid-solid coupling (interactions of SC-CO_2 and coal seam), crack initiation (SC-CO_2 pressure > fracture strength of coal seam), and crack propagation (SC-CO_2 pressure > minimum pressure for crack propagation after fracturing of coal seam).

3.2.1. Basic equations of fluid-solid coupling

During the SC-CO_2 fracturing process, with the continuous injection of SC-CO_2 fluid, the fluid seepage pressure acting on the crack surface increases continuously, which leads to the increase of fluid loss to the coal seam, resulting in the change of stress state in the pores of the coal seam. The change of stress in the coal seam will inevitably lead to

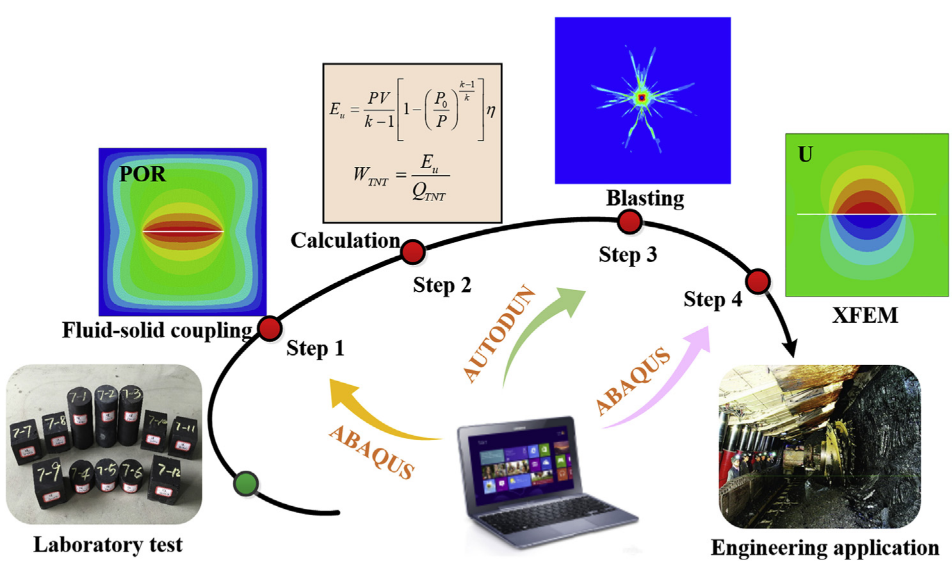

Fig. 3. Analysis procedures.

changes in parameters such as coal seam porosity and fluid seepage velocity, which in turn will affect the change of pore pressure in the seepage field on the crack surface. The fluid seepage and coal seam deformation in the coal seam are mutually constrained. The interaction relationship is called fluid-solid coupling.

The first stage of the simulation uses the ABAQUS analysis platform. ABAQUS is a very powerful finite element software that can provide a variety of methods for simulating crack propagation and solves the problem of fluid-solid coupling. The numerical simulation of SC-CO_2 fracturing stage can be realized by solving the stress equilibrium equation of coal seams and the continuity equation of fluids in ABAQUS numerical simulation (Wang, 2016).

The stress equilibrium equation of coal seam:

$$\int_V (\sigma - mp_w)\delta_\varepsilon dV = \int_S t\delta_V dS + \int_V f\delta_V dV \tag{1}$$

The continuity equation of fluid:

$$\frac{d}{dt}\left(\int_V \psi dV\right) = -\int_S \psi n v_w dS \tag{2}$$

where V refers to the integral space, S refers to the surface of the integral space, σ refers to the effective stress of coal seam, p_w refers to the flow pressure of pore fluid, m refers to the unit matrix vector, δ_ε refers to the virtual strain rate, t refers to the load per unit area, δ_v refers to the virtual velocity field, f refers to the load per unit volume, ψ refers to the porosity of the coal seam, n refers to the normal direction to the surface, v_w refers to the flow rate.

3.2.2. The XFEM model for SC-CO_2 fracturing

The crack initiation and propagation process of coal seam was simulated by XFEM. equation (1) ~ (2) were discretized into matrix equation about stress, strain, displacement, porosity and permeability of coal seam by using ABAQUS implicit solver. The change values of relevant parameters were obtained by solving displacement variables. The unit node displacement was obtained by the continuous displacement field correlation function by XFEM. The XFEM is a new finite element method for solving fracture mechanics problems. It represents the discontinuity of the displacement field by introducing the enrichment function with discontinuous properties in the traditional finite element displacement interpolation function, which usually includes a crack tip progressive displacement function that captures the singular points around the crack tip, and the jump function to represent the displacement jump on the crack surface, the expressions are as follows (Belytschko and Black, 1999):

$$u = \sum_{I=1}^{N} N_I(x)\left[u_I + H(x)a_I + \sum_{\alpha=1}^{4} F_\alpha(x)b_I^\alpha\right] \tag{3}$$

where $N_I(x)$ refers to conventional shape function, u_I refers to displacement vector of continuous part in finite element solution, a_I refers to cracking unit node expansion degree of freedom, $H(x)$ refers to jump function, b_I^α refers to crack tip node expansion degree of freedom, $F_\alpha(x)$ refers to crack tip progressive displacement function, I refers to node set for all nodes in the grid.

When the crack is simulated by XFEM, the crack surface does not need to coincide with the element boundary, and the crack can be expanded in the element. Because the description of the crack surface is completely independent of the mesh, the crack does not need to be reconstructed along any path, greatly reducing the amount of computation. Therefore, this simulation uses the XFEM to construct an extended model of SC-CO_2 fracturing.

3.2.3. Initiation and propagation of cracks

Based on simulation experience (Cai et al., 2004), the norm of maximum principal stress was selected for crack initiation in the numerical simulation of SC-CO_2 fracturing. Once the SC-CO_2 pressure exceeds the critical maximum principal stress of the coal seam, damage is initiated, and fracturing of coal seam is observed. The equation of the norm of maximum principal stress is:

$$f = \left\{\frac{\langle\sigma_{\max}\rangle}{\sigma_{\max c}}\right\} \tag{4}$$

where σ_{maxc} refers to the critical maximum principal stress of the coal seam. The symbol $< \ >$ indicates that cracking damage does not occur when the coal seam is purely compressed, in other words, when $\sigma_{\max} < 0$, $< \sigma_{\max} > \ = 0$, and when $\sigma_{\max} \geq 0$, $< \sigma_{\max} > \ = \sigma_{\max}$.

Crack propagation during SC-CO_2 fracturing is a complicated process and the categories of cracks cannot be predicted. Hence, the concept of energy release rate (i.e., the B-K norm) was introduced into the norm of maximum principal stress in order to predict crack propagation (Benzeggagh and Kenane, 1996). The expression of BK criterion is as follows:

$$G_n^C + (G_s^C - G_n^C)\left(\frac{G_S}{G_T}\right)^\eta = G^C \tag{5}$$

Where $G_S = G_s + G_t$, $G_T = G_n + G_s$, $G_n{}^C$ is the critical strain energy release rate of normal fracture, N/mm; $G_s{}^C$ and $G_t{}^C$ are the critical energy release rates of two tangential fractures, N/mm, BK criterion considers $G_s{}^C = G_t{}^C$, η is a constant related to the properties of the material itself; G^C is the critical fracture energy release rate of the composite crack, N/mm. Here, $G_n{}^C = 16$N/mm, $G_s{}^C = G_t{}^C = 18$N/mm, $\eta = 2.284$.

To reduce calculation, a 2D model with the size of $20 \times 20\,m^2$ was used (see Fig. 4). The fracturing borehole was placed in the central part of the model. As the SC-CO_2 fluid flows through the initial cracks, the initial cracks do not deflect and tangential work by the fluid pressure in the initial cracks on the fracturing surface was significantly lower than that on the non-fracturing area. The diameter of the fracturing borehole is characterized by the length of initial cracks ($d = 100$ mm). To minimize the interferences by the stress difference, crustal stresses in the horizontal and vertical directions were aligned. Based on simulation of the fluid injection function, the injection of SC-CO_2 fluid into the fracturing coal seams was achieved. The simulation period was 180 s.

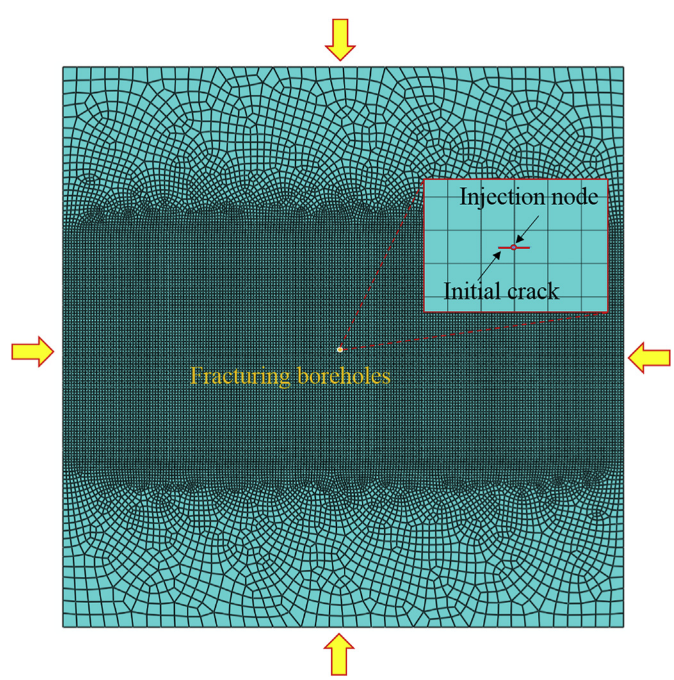

Fig. 4. Fluid-solid coupling model.

3.3. TNT equivalence of CO_2 phase transition induced fracturing

Once the injection of the SC-CO_2 fluid was terminated, the CO_2 pressure fell dramatically, and the SC-CO_2 transitioned from the supercritical state to the gaseous state, resulting in severe swelling and blasting impacts from the high energy CO_2. The total released blast energy at the phase transition of SC-CO_2 is given by (Gel'Fand et al., 1988):

$$E_g = \frac{PV}{k-1}\left[1-\left(\frac{P_0}{P}\right)^{\frac{k-1}{k}}\right] \tag{6}$$

where E_g refers to the total energy released by phase transition, P refers to the CO_2 pressure at the crack before phase transition, P_0 refers to the minimum pressure required for crack propagation, V refers to the crack volume before phase transition of CO_2, and k refers to the adiabatic coefficient where $k = 1.295$ for CO_2

The process of the energy released by phase transition exists the phenomenon of filtration and loss, not all energy is released in the form of shock waves. To more accurately calculate the energy used for expansion cracking, the energy utilization rate is introduced:

$$E_u = \eta \times E_g \tag{7}$$

Where E_u is the useful energy in the total energy released by phase transition, and η is the energy utilization rate. Here $\eta = 0.9$, its value mainly refers to the loss of energy in the BLEVE phenomenon (Casal, 2018).

Therefore, the TNT equivalence of CO_2 phase transition induced fracturing (W_{TNT}) is:

$$W_{TNT} = \frac{E_u}{Q_{TNT}} \tag{8}$$

where Q_{TNT} refers to the blast energy of 1 kg explosive, which is 4250 kJ/kg in this case.

3.4. Pressure-time history curves of blast loads

The AUTODYN software was employed to determine the blast load caused by the CO_2 phase transition induced fracturing. The AUTODYN is an explicit finite element analysis software and is a module of ANSYS. Because it can provide the material model of high-energy explosives and the equation of state of various explosives, and accurately simulate the transient response history of the entire explosion, it has unique advantages in solving highly nonlinear dynamic problems such as collision impact, explosion, and stamping (Sun et al., 2012). As the simulation doesn't involve monitoring of deformation and stress, the model size was set as $2 \times 2\,m^2$ and the explosive equivalence was determined by the TNT equivalence in Section 3.3. The model involves air, TNT, and coal seam, where air and TNT were determined by the Euler algorithm and coal seam was determined by the Lagrange algorithm. The pressure-time history curves of blast loads on areas near the borehole wall were obtained by coupling calculations, as shown in Fig. 5.

3.5. Numerical model for the CO_2 phase-transition induced fracturing stage

To guarantee the comparability of fracturing effects, the numerical model for the CO_2 phase transition induced fracturing stage was also established by XFEM on ABAQUS and its basic conditions were aligned with that of the model for the SC-CO_2 fracturing stage. The cracks at the SC-CO_2 fracturing stage were pre-transferred to the new model and the pressure-time history curves of blast loads obtained in Section 3.4 were applied on the crack propagation surface to achieve numerical simulations of the CO_2 phase-transition induced fracturing stage.

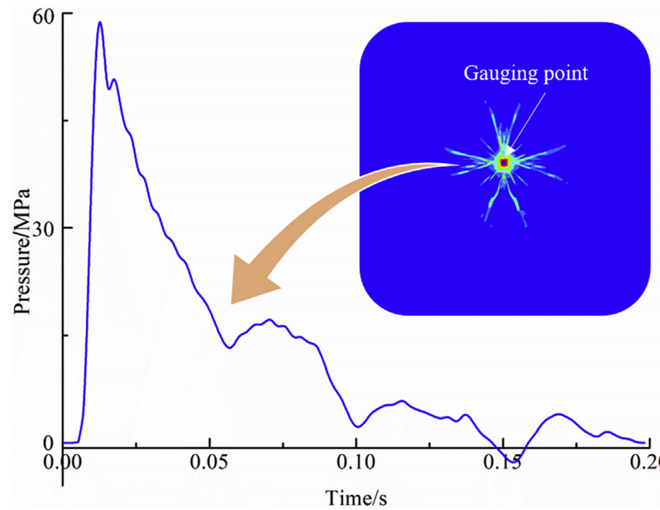

Fig. 5. The pressure-time history curves of blast loads.

3.6. Verification of numerical simulations

The proposed numerical simulation of SC-CO_2 fracturing was verified using the experimental results on the true triaxial stress testing of sandstone using SC-CO_2 fracturing conducted by Zhang et al. (2017b). The experiment adopted SC-CO_2 fracturing simulation experiment system, which consisted of five parts: a triaxial loading system, a thermotank, a carbon dioxide plunger pump, a CO_2 heating unit and a temperature pressure data collection device. The test piece was made of $200 \times 200 \times 200\,mm^3$ sandstone, and a borehole with a hole diameter of 20 mm and a depth of 110 mm was drilled in the middle of the test piece to simulate the fracturing borehole. The SC-CO_2 fracturing experiment was realized by controlling the temperature and pressure of CO_2.

A numerical model corresponding to the above test conditions was established and the simulation parameters was set according to the specific conditions of the test. Therein, the elastic modulus, the Poisson ratio, and the tensile strength of the sandstone were 36 GPa, 0.24, and 4.1 MPa, respectively. The vertical crustal stress of the model was 12 MPa, the maximum and minimum horizontal crustal stress on the model were 10 MPa and 8 MPa, respectively, and the injection rate of the SC-CO_2 fluid at 10 MPa and 60 °C was 30 mL/min.

The pre-cracking direction of the fracture borehole in the numerical model was determined in lab tests to be according to the crack initiation direction. The numerical simulation results were compared with the laboratory test results (see Fig. 6). As can be observed, the dynamic propagation of cracks during SC-CO_2 fracturing was consistent with previous studies, indicating the excellent reliability and feasibility of the proposed numerical simulation of SC-CO_2 fracturing.

3.7. Comparative analysis of SC-CO_2 fracturing and hydraulic fracturing

In order to compare the difference between SC-CO_2 fracturing and hydraulic fracturing, the numerical model of SC-CO_2 fracturing and hydraulic fracturing was constructed by the proposed simulation method. The simulation method of SC-CO_2 fracturing adopted staged numerical simulation while the simulation method of hydraulic fracturing was the same as the first stage of SC-CO_2 fracturing. The fluid permeability coefficient, fluid viscosity and fluid density of SC-CO_2 fracturing were 1×10^{-5} m/s, 7×10^{-5} Pas and 780 kg/m^3, respectively. While these values for hydraulic fracturing were 1×10^{-7} m/s, 1×10^{-3} Pas and 980 kg/m^3, respectively. The basic parameters of these two models were the same, and the horizontal and vertical crustal stresses on the model were both 12 MPa.

The comparison of fracturing effects between SC-CO_2 fracturing and

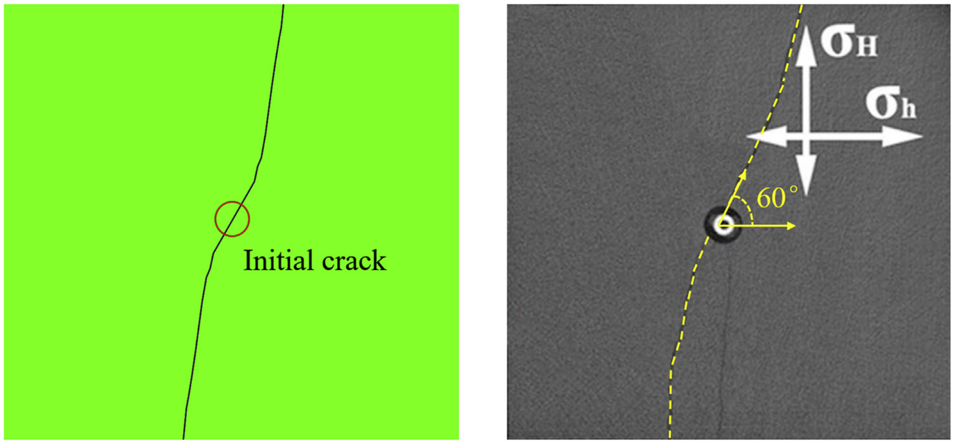

(a) Numerical simulation results (b) Experimental results

Fig. 6. Comparison of numerical simulation and experimental results.

Table 1
Comparison of fracturing effects between SC-CO_2 fracturing and hydraulic fracturingTable 1 Comparison of fracturing effects between SC-CO_2 fracturing and hydraulic fracturing.

Fracturing method	Crack initiation pressure/MPa	Crack propagation length/m	Crack propagation width/mm
SC-CO_2 fracturing	32.3	13.0	10.2
hydraulic fracturing	43.5	10.8	4.0

Note: the crack propagation length is equal to two times of the crack propagation radius.

hydraulic fracturing was shown in Table 1. From the aspect of crack initiation pressure, the initiation pressure of SC-CO_2 fracturing was 32.3 MPa, the initiation pressure of hydraulic fracturing was 43.5 MPa, and the initiation pressure of SC-CO_2 fracturing was lower than that of hydraulic fracturing, because the SC-CO_2 fluid has strong diffusion ability and is more likely to penetrate into micro cracks and pores, thus causing the crack initiation pressure to decrease. From the aspect of crack propagation, the length and width of crack propagation of SC-CO_2 fracturing were 13.0 m and 10.2 mm respectively, while these values for hydraulic fracturing were 10.8 m and 4.0 mm respectively, the SC-CO_2 fracturing had larger crack propagation length and width, and the fracturing effect was better, which was due to the further expansion of the crack caused by the phase-transition of CO_2 during the SC-CO_2 fracturing process. Therefore, the crack initiation pressure of SC-CO_2 fracturing was lower than that of hydraulic fracturing, and the fracturing effect was better than that of hydraulic fracturing, thus SC-CO_2 fracturing had obvious advantages in fracturing.

4. Staged simulations of crack propagation

Crack propagations at the SC-CO_2 fracturing stage and the CO_2 phase-transition induced fracturing stage were investigated based on staged simulations. In these simulations, the working conditions in coal seams with a depth of 500 m were applied, the horizontal and vertical crustal stress on the model were 12 MPa, the stratum pore pressure was 5 MPa, and SC-CO_2 at 20 MPa and 50 °C was used as the fracturing fluid.

4.1. Crack propagation length

The crack propagation length is a direct indicator of the fracturing effects of coal seam. The fracturing state during SC-CO_2 fracturing of coal seam is shown in Fig. 7. PHILSM in Fig. 7 refers to the displacement function used to describe the crack surface, according to which the crack propagation length can be obtained, and the crack propagation length was equal to two times of the crack propagation radius. It can be seen that cracks propagated further during the CO_2 phase-transition induced fracturing stage: the crack propagation lengths at the end of the SC-CO_2 fracturing stage (L_1) and CO_2 phase transition induced fracturing stage (L_2) were 9.6 m and 13.0 m, respectively.

4.2. Maximum width of propagated cracks

The width of cracks is another indicator of fracturing effects in coal seams. Considering that the closure of cracks at the end of the SC-CO_2 fracturing stage leads to significantly reduced crack width, the maximum crack widths at the two fracturing stages was statistically analyzed in the simulation, as shown in Fig. 8. As can be observed, the maximum crack widths at the SC-CO_2 fracturing stage and the CO_2 phase-transition induced fracturing stage were 4.0 mm and 10.2 mm, respectively, indicating that crack width increased significantly during the CO_2 phase-transition induced fracturing stage. Additionally, the width increase was observed for existing cracks, while the widths of new cracks were significantly smaller than those of existing cracks.

These results demonstrated the key role of the SC-CO_2 fracturing stage and the CO_2 phase-transition induced fracturing stage in the overall fracture process: cracks in the coal seam were initiated and propagated during the SC-CO_2 fracturing stage, while the cracks were broadened, and new cracks were generated at the CO_2 phase-transition induced fracturing stage. Therefore, staged numerical simulations of SC-CO_2 fracturing play a key role in the full understanding of the SC-CO_2 fracture mechanism.

5. Discussion

In practical applications, the injection rate of the SC-CO_2 fluid is a controllable factor with significant effects on the fracturing process (Harpalani and Mitra, 2010; Wang et al., 2016). To understand the effects of the injection rate of SC-CO_2 fluid on fracturing effects, the injection rates of the SC-CO_2 fluid were set to be $5 \times 10^{-5}\,m^2/s$, $8 \times 10^{-5}\,m^2/s$, and $1 \times 10^{-4}\,m^2/s$, respectively and working conditions in coal seams with a depth of 500 m were applied.

The crack propagation lengths at different injection rates of SC-CO_2 are illustrated in Fig. 9. As is evident, the crack propagation length increased with the injection rate of SC-CO_2. Specifically, the crack propagation lengths after the SC-CO_2 fracturing stage were 5.6 m, 8.2 m, 9.6 m at the injection rates of the SC-CO_2 fluid = $5 \times 10^{-5}\,m^2/s$,

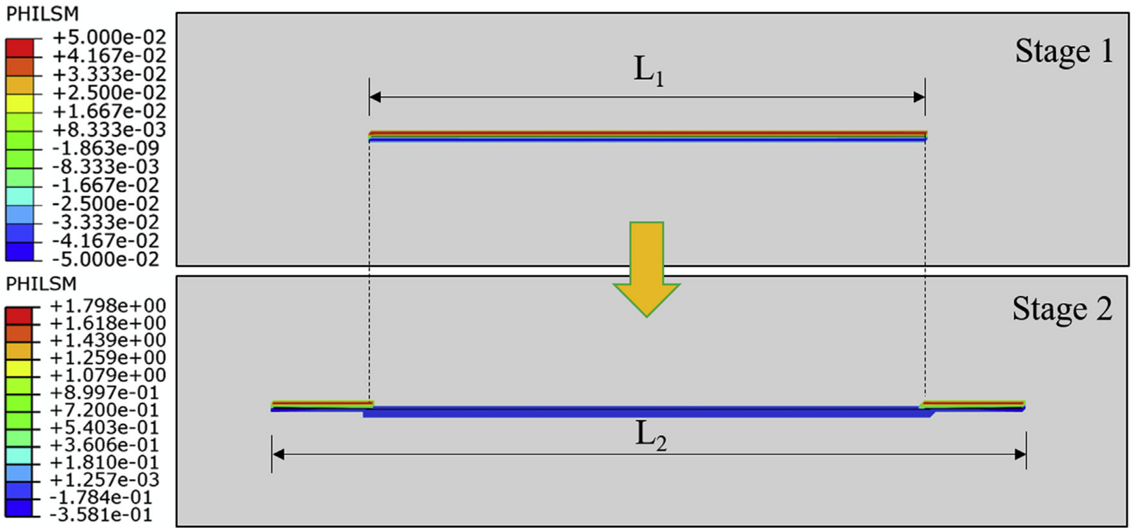

Fig. 7. Fracturing state in the SC-CO_2 fracturing.

8×10^{-5} m^2/s, 1×10^{-4} m^2/s, respectively, while the crack propagation lengths after the CO_2 phase-transition induced fracturing stage were 7.4 m, 11.0 m, 13.0 m at the injection rates of the SC-CO_2 fluid = 5×10^{-5} m^2/s, 8×10^{-5} m^2/s, 1×10^{-4} m^2/s, respectively. As the injection rate of SC-CO_2 is increased, the fluid pressure increases, resulting in crack conduction by the SC-CO_2 fluid and enhanced fracturing effects. Therefore, the fracturing effects can be enhanced by increasing the injection rate of SC-CO_2 in practical applications.

The maximum crack widths at different injection rates of SC-CO_2 are illustrated in Fig. 10. As can be observed, the maximum crack width increased with the injection rate of SC-CO_2. Specifically, the maximum crack widths were 3.9 mm, 7.0 mm, 10.2 mm at injection rates of the SC-CO_2 fluid of 5×10^{-5} m^2/s, 8×10^{-5} m^2/s, 1×10^{-4} m^2/s, respectively. Thus, the increasing amplitude of the maximum crack width at an injection rate of 1×10^{-4} m^2/s was large. In practical applications, the optimized injection rate could be determined according to the working conditions and production requirements.

In summary, the injection rate of the SC-CO_2 fluid has a significant effect on crack propagation length and width of the coal seam fractures. As different industrial applications require different fracturing effects, optimized fracturing parameters in the engineering design shall be determined based on their cost and their technical feasibility.

In the process of constructing the numerical model, the coal seam is assumed to be an isotropic material, and the fracturing effect in the depth direction of the fracturing borehole is assumed to be the same, thus the practical problem is simplified into a plane problem, and the plane perpendicular to the depth of the borehole is taken as the research object. Because the fracturing borehole depth in coal mine is small (generally less than 8 m), it is a certain reliability to simplify the actual working condition of the SC-CO_2 fracturing coal seams to the plane problem. This simulation method can be applied to study the crack propagation law of SC-CO_2 fracturing and the influence of various factors on the crack propagation under the condition of small borehole depth. The research results have certain guiding significance for fully understanding the mechanism of SC-CO_2 fracturing and the design of engineering parameters. When the fracturing borehole depth is large, the anisotropy of the coal seam is obvious, and the fracturing effect in the depth direction of the fracturing borehole is quite different, it is

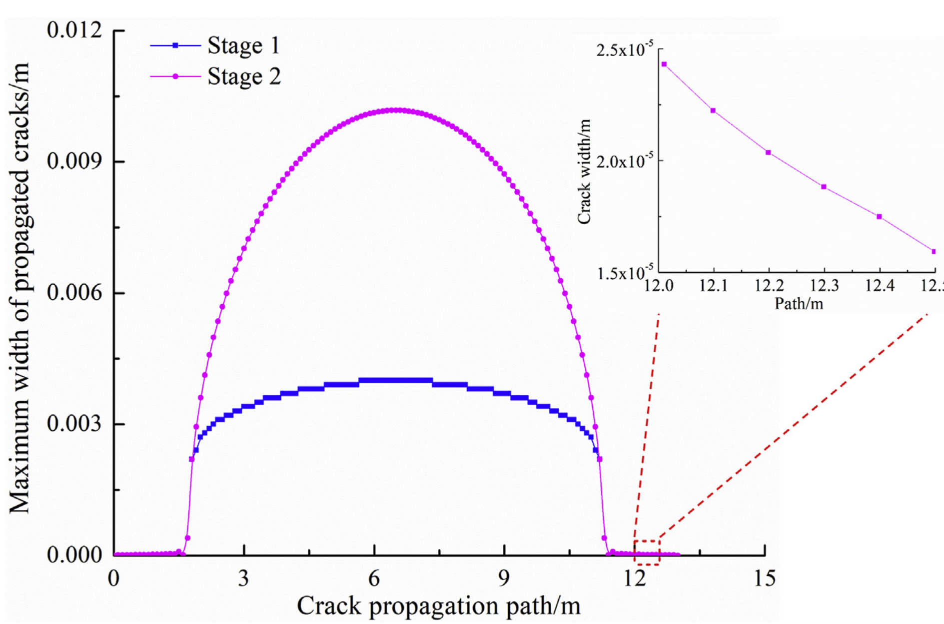

Fig. 8. Maximum width of cracks at the two fracturing stages.

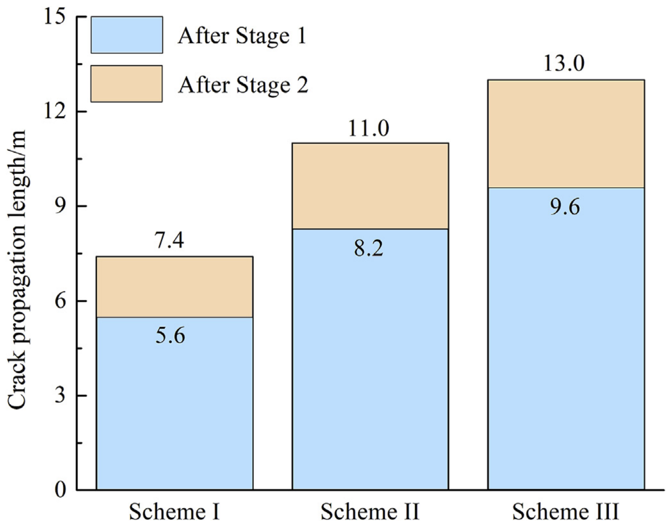

Fig. 9. Crack propagation lengths at different injection rates of SC-CO_2.

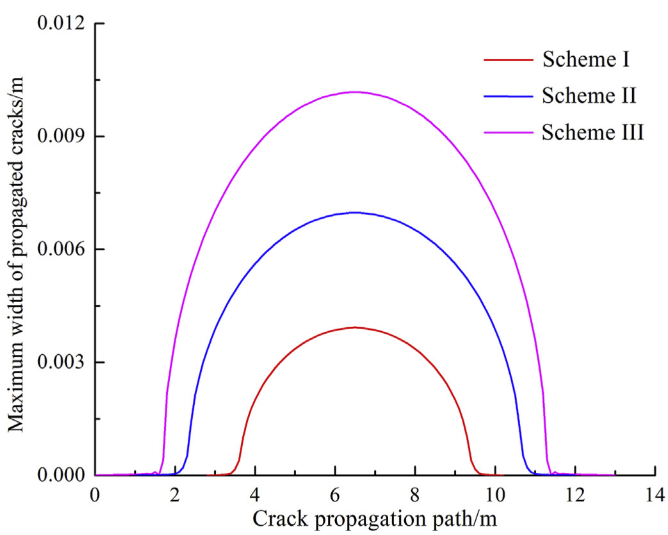

Fig. 10. Maximum crack widths at different injection rates of SC-CO_2.

necessary to exhibit the effect of SC-CO_2 fracturing in space, and the two-dimensional plane model is no longer applicable, so the future research focus will gradually develop to the three-dimensional model to achieve more accurate numerical simulation studies.

6. Conclusions

In the present study, the SC-CO_2 fracturing process was considered in two stages and a staged numerical simulation of the SC-CO_2 fracture of coal seams was proposed, based on the XFEM finite element code. The following conclusions were drawn on the basis of the investigation:

(1) The SC-CO_2 fracturing process was considered as being divided into the SC-CO_2 fracturing stage and the CO_2 phase-transition induced fracturing stage. During the early stage of fracturing, the SC-CO_2 fluid can readily enter micro-pore cracks, due to its low viscosity and high diffusivity, which results in the initiation and propagation of cracks. During the later stage of fracturing, the SC-CO_2 transitions from the supercritical state to the gaseous state, which results in a dramatic expansion of the CO_2 in a short period of time. The severe impact of this transition leads to further propagation of the cracks.

(2) Based on the extended finite element method, a staged numerical simulation of the SC-CO_2 fracturing is proposed. A fluid-solid coupling model was developed using the Soil module in ABAQUS software for the simulation of the SC-CO_2 fracturing stages. Furthermore, the blast loads induced by phase transition of the CO_2 were introduced into the SC-CO_2 model for simulation of the CO_2 phase-transition induced fracture stage.

(3) Cracks in the coal seam are initiated and propagated at the SC-CO_2 fracture stage, and the cracks broaden, and new cracks are generated during the CO_2 phase-transition induced fracturing stage.

Acknowledgments

This research was funded by the National Key R & D Program of China [grant number 2018YFC0604704], the National Science Fund for Distinguished Young Scholars [grant number 51725403] and the China Scholarship Council [grant number 201806420060].

Appendix A. Supplementary data

Supplementary data to this article can be found online at https://doi.org/10.1016/j.jngse.2019.03.021.

References

Belytschko, T., Black, T., 1999. Elastic crack growth in finite elements with minimal remeshing. Int. J. Numer. Methods Eng. 45, 601–620.

Benzeggagh, M., Kenane, M., 1996. Measurement of mixed-mode delamination fracture toughness of unidirectional glass/epoxy composites with mixed mode bending apparatus. Compos. Sci. Technol. 56, 439–449.

Brownlow, J., Yelderman, J., James, S., 2017. Spatial risk analysis of hydraulic fracturing near abandoned and converted oil and gas wells. Gr. Water 55, 268–280.

Cai, M., Kaiser, P., Tasaka, Y., Maejima, T., Morioka, H., Minami, M., 2004. Generalized crack initiation and crack damage stress thresholds of brittle rock masses near underground excavations. Int. J. Rock Mech. Min. 41, 833–847.

Camarillo, M., Domen, J., Stringfellow, W., 2016. Physical-chemical evaluation of hydraulic fracturing chemicals in the context of produced water treatment. J. Environ. Manag. 183, 164–174.

Cao, Y., Zhang, J., Zhai, H., Fu, G., Tian, L., Liu, S., 2017. CO_2 gas fracturing: a novel reservoir stimulation technology in low permeability gassy coal seams. Fuel 203, 197–207.

Casal, J., 2018. Evaluation of the Effects and Consequences of Major Accidents in Industrial Plants, second ed. Elsevier, Netherlands.

Dong, X., Karrech, A., Basarir, H., Elchalakani, M., Seibi, A., 2018. Energy dissipation and storage in underground mining operations. Rock Mech. Rock Eng. 4, 1–17.

Er, V., Babadagli, T., Xu, Z., 2010. Pore-Scale Investigation of the matrix − fracture interaction during CO_2 injection in naturally fractured oil reservoirs. Energy Fuel. 24, 295–317.

Estrada, J., Bhamidimarri, R., 2016. A review of the issues and treatment options for wastewater from shale gas extraction by hydraulic fracturing. Fuel 182, 292–303.

Gel'Fand, B., Frolov, S., Bartenev, A., 1988. Calculation of the rupture of a high-pressure reactor vessel. Combust. Explo. Shock+. 24, 488–496.

Harpalani, S., Mitra, A., 2010. Impact of CO_2 injection on flow behavior of coalbed methane reservoirs. Transport Porous Media 82, 141–156.

Huang, B., Li, P., Ma, J., Chen, S., 2014. Experimental investigation on the basic law of hydraulic fracturing after water pressure control blasting. Rock Mech. Rock Eng. 47, 1321–1334.

Ishida, T., Aoyagi, K., Niwa, T., Chen, Y., Murata, S., Chen, Q., Nakayama, Y., 2012. Acoustic emission monitoring of hydraulic fracturing laboratory experiment with supercritical and liquid CO_2. Geophys. Res. Lett. 39, L16309.

Jia, Y., Lu, Y., Elsworth, D., Fang, Y., Tang, J., 2018. Surface characteristics and permeability enhancement of shale fractures due to water and supercritical carbon dioxide fracturing. J. Pet. Sci. Eng. 165, 284–297.

Jiang, B., Wang, L., Lu, Y., Wang, C., Ma, D., 2016. Combined early warning method for rockburst in a Deep Island, fully mechanized caving face. Arab. J. Geosci. 9, 743.

Li, H., Wang, Z., Chen, X., Zhao, L., Zhou, D., 2017. Optimization of borehole layout parameters based on fracturing technology of liquid CO_2 phase. Coal Geol. Explor. 45, 31–37.

Luek, J., Gonsior, M., 2017. Organic compounds in hydraulic fracturing fluids and wastewaters: a review. Water Res. 123, 536–548.

Martynov, S., Brown, S., Mahgerefteh, H., Sundara, V., Chen, S., Zhang, Y., 2014. Modelling three-phase releases of carbon dioxide from high-pressure pipelines. Process Saf. Environ. 92, 36–46.

Middleton, R., Carey, B., Currier, R., Hyman, J., Kang, Q., Karra, S., Joaquín, J., Porter, M., Viswanathan, H., 2015. Shale gas and non-aqueous fracturing fluids: opportunities and challenges for supercritical CO_2. Appl. Energy 147, 500–509.

Sun, J., Fan, H., Wei, C., Jiang, T., Zhao, Y., 2012. Numerical simulation on foam ceramic blasting block device under the action of explosion transform. Saf. Sci. 50, 588–592.

Vishal, V., 2017. In-situ disposal of CO_2: liquid and supercritical CO_2, permeability in coal

at multiple down-hole stress conditions. J. CO2 Util. 17, 235–242.
Wang, H., 2016. Numerical investigation of fracture spacing and sequencing effects on multiple hydraulic fracture interference and coalescence in brittle and ductile reservoir rocks. Eng. Fract. Mech. 157, 107–124.
Wang, J., Sun, B., Wang, Z., Zhang, J., 2017a. Study on filtration patterns of supercritical CO_2 fracturing in unconventional natural gas reservoirs. Greenh. Gases 7, 1126–1140.
Wang, L., Yao, B., Xie, H., Winterfeld, P., Kneafsey, T., Yin, X., Wu, Y., 2017b. CO_2 injection-induced fracturing in naturally fractured shale rocks. Energy 139, 1094–1110.
Wang, Y., Li, X., Zhang, B., 2016. Numerical modeling of variable fluid injection-rate modes on fracturing network evolution in naturally fractured formations. Energies 9, 414.
Xu, J., Jiang, J., Xu, N., Liu, Q., Gao, Y., 2017. A new energy index for evaluating the tendency of rockburst and its engineering application. Eng. Geol. 230, 46–54.
Yang, T., Nie, B., Yang, D., Zhang, R., Zhao, C., 2012. Experimental research on displacing coal bed methane with supercritical CO_2. Saf. Sci. 50, 899–902.
Yang, Z., Yi, L., Li, X., Chen, Y., Sun, J., 2018. Model for calculating the wellbore temperature and pressure during supercritical carbon dioxide fracturing in a coalbed methane well. J. CO2 Util. 26, 602–611.
Zhang, X., Lu, Y., Tang, J., Zhou, Z., Liao, Y., 2017a. Experimental study on fracture initiation and propagation in shale using supercritical carbon dioxide fracturing. Fuel 190, 370–378.
Zhang, Y., Zhang, Z., Sarmadivaleh, M., Lebedev, M., Barifcani, A., Yu, H., Iglauer, S., 2017b. Micro-scale fracturing mechanisms in coal induced by adsorption of supercritical CO_2. Int. J. Coal Geol. 175, 40–50.
Zhou, J., Liu, G., Jiang, Y., Xian, X., Liu, Q., Zhang, D., Tan, J., 2016. Supercritical carbon dioxide fracturing in shale and the coupled effects on the permeability of fractured shale: an experimental study. J. Nat. Gas Sci. Eng. 36, 369–377.
Zhou, Y., Liu, Z., Huang, Q., Wang, F., Zhang, D., 2014. Small scale experiments of CO_2 boiling liquid expanding vapor explosion in injection pipes. Energy Procedia 61, 782–786.
Zou, Y., Li, N., Ma, X., Zhang, S., Li, S., 2018. Experimental study on the growth behavior of supercritical CO_2-induced fractures in a layered tight sandstone formation. J. Nat. Gas Sci. Eng. 49, 145–156.